Rapidly convergent spectral representations for periodic Green functions

Vitaliy Lomakin[1], Derek Van Orden[1]

[1]University of California, San Diego
9500 Gilman Dr., La Jolla, CA 92093, USA
E-mail: vitaliy@ece.ucsd.edu, derekvanorden@gmail.com

Abstract

Spectral representations for the Green function for 2D and 3D configurations with 1D periodicities are introduced. The representations rely on the expansion of the Green function in terms of the continuous longitudinal spectrum. These representations allow obtaining the Green functions in terms of a small number of direct source contributions, a small number of pole (Floquet mode) contributions, and a rapidly convergent integral that can be evaluated using quadrature rules with a small number of nodes. The presented schemes work seamlessly even for small/vanishing source-observer separations as well as for large periodicities.

1. Introduction

Efficient methods for computing Green's functions for periodic electromagnetic problems are important to enable the use of integral equation methods, to compute fields radiated and scattered from periodic configurations, and to study the dispersion properties of periodic structures. It is well known that representations of periodic Green functions via direct spatial summations are extremely slowly convergent. Summations in terms of Floquet series suffer slow convergence problems in the important case where the observer resides near a periodic structure. Several approaches, including the Ewald approach [1-3] and the perfectly matched layer (PML) method [4,5] have been suggested to lead to rapidly convergent representations. The Ewald approach, while leading to exponential convergence, can result in high-frequency breakdown and requires choosing the optimal splitting parameter, which may be not straightforward and may lead to efficiency restrictions. The PML method applied to 3D configurations has to be combined with the Ewald approach and may be hard to use.

Here, we introduce a novel method for computing periodic Green functions. The method is based on the alternative Green function representation formalism [6] and involves the longitudinal (vertical) spectrum representation with transverse (horizontal) 1D periodic Green's function available in closed form. These representations lead to exponential computational convergence regardless of the source-observer separation. The resulting Green functions explicitly satisfy the radiation conditions without a need to define any branch cuts associated with Floquet mode wavenumbers thus simplifying their use. In this initial study, we consider Green functions for 2D and 3D problems with a 1D periodicity. Generalizations to layered medium configuration are also discussed.

2. Problem formulation

Consider a 1D array of sources along the x axis as shown in Fig. 1. The sources are linear and point for 2D and 3D problems, respectively. The periodicity of the array is L and the sources have a linear phase shift $e^{-jk_{x0}nL}$, where n is an integer and a possibly complex k_{x0} determines the phase shift. The time dependence $e^{j\omega t}$ is suppressed.

Electromagnetic fields radiated by this array can be found from the periodic Green functions

$$G^{2D}(\mathbf{r}) = \sum_{n=-\infty}^{\infty} \exp(-jk_{x0}nL)\frac{j}{4}H_0^{(2)}(kR_n); \qquad G^{3D}(\mathbf{r}) = \sum_{n=-\infty}^{\infty} \exp(-jk_{x0}nL)\frac{\exp(-jkR_n)}{4\pi R_n} \tag{1}$$

given with respect to the source at one of the unit cells as shown in Fig. 1. In (1), $R_n = |\mathbf{r} - \mathbf{r}_n|$ is the distance from the observer to the source at the location $\mathbf{r}_n$, whereas G^{2D} and G^{3D} are 2D and 3D periodic Green functions, respectively. The function G^{3D} is axially symmetric and hence depends only on x and $\rho = (x^2 + y^2)^{1/2}$. For lossless media the series in Eq. (1) converges extremely slowly.

The periodic Green functions can also be represented in terms of the following Floquet mode expansions

$$G^{2D}(\mathbf{r}) = \sum_{n=-\infty}^{\infty} \exp(-jk_{xn}x)\frac{\exp(-jk_{tn}|z|)}{2jk_{tn}}; \qquad G^{3D}(\mathbf{r}) = \sum_{n=-\infty}^{\infty} \exp(-jk_{xn}x)\frac{j}{4}H_0^{(2)}(k_{tn}\rho) \tag{2}$$

where $k_x = k_{x0} + 2\pi n/L$ is the transverse wavenumber, $k_{tn} = (k^2 - k_{xn}^2)^{1/2}$ is the longitudinal wavenumber with $k = \omega/c$, and $\mathrm{Im}\{k_{tn}\} < 0$. The sum (2) converges exponentially fast when $|z|, \rho > 0$. On the other hand, in the important case $|z| = \rho \to 0$, the summation in (2) converges extremely slowly. Therefore, alternative rapidly convergent representations for G^{2D} and G^{3D} are to be developed.

3. Spectral representations

The field can be given via an alternative representation in terms of the longitudinal spectrum [6]

$$G^{2D}(\mathbf{r}) = \frac{1}{2\pi}\int_{-\infty}^{\infty} dk_t \exp(-jk_t z) g_x(x;k_x); \qquad G^{3D}(\mathbf{r}) = \frac{1}{2\pi}\int_0^{\infty} dk_t k_t J_0(k_t\rho) g_x(x;k_x) \tag{3}$$

Here, $J_0(\cdot)$ is the Bessel function, $k_x = (k^2 - k_t^2)^{1/2}$ is the wavenumber in the x direction, and $g_x(x;k_x)$ is the periodic Green function of the spectral 1D problem. This function is given in a closed form by

$$g_x(x;k_x) = \frac{1}{2jk_x}\left(\frac{\exp(-jk_x|x|)}{1-\exp(-j(k_x-k_{x0})L)} - \frac{\exp(jk_x|x|)}{1-\exp(j(k_x+k_{x0})L)}\right) \tag{4}$$

The function $g_x(x;k_x)$ has poles $k_{tpn} = \left(k^2 - (k_{x0} + 2\pi n/L)^2\right)^{1/2}$ in the complex k_x plane (Fig. 2). For lossless configurations, these poles form pairs with opposite sign on either the imaginary or real axis. The poles on the imaginary and real axis correspond to Floquet modes that are evanescent or propagating in the z direction, respectively. The Green function $g_x(x;k_x)$ does not have any branch points as a function of k_t even though k_x does. The mathematical reason for the absence of the branch points is that $g_x(x;k_x)$ is an even function in terms of k_x. The physical reason is that the spectral 1D periodic problem is essentially a "closed domain" problem so that no radiation condition should be satisfied. The function $g_x(x;k_x)$ decays exponentially for large $|k_x|$ (and hence for large $|k_z|$) for $|x| > 0$. The integration path in (3) follows the real axis above or below the poles k_{tpn} depending on the pole locations, which, for given k and L, are determined by k_{x0} and n (see the complex plane in Fig. 2).

Due to the decay of $g_x(x;k_x)$, the representation (3) is exponentially convergent even when $|z| = \rho = 0$ provided that $|x| > 0$. For numerical implementation the convergence of the integrals (3) can be further improved by explicitly extracting the contribution of a certain number of sources in and around the unit cell of interest and by deforming the integration path in (3) to the steepest descent path (SDP) defined as in [6] (see Fig. 2)

$$\begin{aligned}
G^{2D}(\mathbf{r}) &= \sum_{n=-(N_d-1)/2}^{(N_d-1)/2} \exp(-jk_{x0}nL)\frac{j}{4}H_0^{(2)}(kR_n) + \sum_{n=1}^{N_p} j \operatorname*{Res}_{k_t=k_{tpn}}\left\{\exp(-jk_t z)g_x(x;k_x)\right\} \\
&\quad + \frac{1}{2\pi}\int_{\mathrm{SDP}}\left(\frac{\exp(jk_{x0}LN_d)\exp\left(-jk_x(LN_d+x)\right)}{1-\exp(-j(k_x-k_{x0})L)} + \frac{\exp(-jk_{x0}LN_d)\exp\left(-jk_x(LN_d-x)\right)}{1-\exp(-j(k_x+k_{x0})L)}\right)\frac{\exp(-jk_t z)}{2jk_x}dk_t \\
G^{3D}(\mathbf{r}) &= \sum_{n=-(N_d-1)/2}^{(N_d-1)/2} \exp(-jk_{x0}nL)\frac{\exp(-jkR_n)}{4\pi R_n} + \sum_{n=1}^{N_p} j \operatorname*{Res}_{k_t=k_{tpn}}\left\{\frac{k_t J_0(k_t\rho)}{2jk_x}g_x(x;k_x)\right\} \\
&\quad + \frac{1}{2\pi}\int_{\mathrm{SDP}}\left(\frac{\exp(jk_{x0}LN_d)\exp\left(-jk_x(LN_d+x)\right)}{1-\exp(-j(k_x-k_{x0})L)} + \frac{\exp(-jk_{x0}LN_d)\exp\left(-jk_x(LN_d-x)\right)}{1-\exp(-j(k_x+k_{x0})L)}\right)\frac{k_t J_0(k_t\rho)}{2jk_x}dk_t
\end{aligned} \tag{5}$$

Here, the first summations represent contributions due to N_d sources in and around the origin (Fig. 1). The second summations represent contributions of N_p poles crossed while the integration path deformation. The SDP integrals represent the contribution of the rest of the sources. The integrands in Eq. (5) have branch points associated with $k_x = (k^2 - k_t^2)^{1/2}$ but they can be avoided by variable transformations. Provided that $\mathrm{Im}\{k_x\} < 0$, the integrands in (5) decay rapidly with $|k_t| > k$. Moreover, the integrands are smooth functions of k_t, except maybe of special cases where the poles reside near the saddle point. However, in the latter case, they can be easily smoothed using techniques in [6]. Therefore, the integrals can be evaluated using a quadrature rule with a small number of nodes. Typically, only a small number of poles N_p is needed to be taken into account and a small N_d is sufficient to render a sufficient convergence.

The representation in (5) is efficient for any x within the unit cell (even for $|x|=0$) and for any practical periodicities L (whether for subwavelength L or for L of several wavelengths).

4. Numerical results

To exemplify the performance of the introduced schemes, Fig. 3(a) and (b) show the Green functions along the horizontal line $0.001L < x < 0.5L$ for $k_{x0} = (0.8 - 0.0001j)k$ for very small $|z| = \rho = 10^{-4}\lambda$ for three values of $L = 0.2\lambda, 1.2\lambda, 2.2\lambda$ (with $\lambda = 2\pi/k$ the wavelength). For the results evaluated via (5), $N_d = 7$, N_p was 2 for $L = 0.2\lambda$, $L = 1.2\lambda$ and 4 for $L = 2.2\lambda$. The integrals in (5) were evaluated using the 9 quadrature nodes. These results were compared with results obtained via (2) with 20000 summation terms. It is evident that the results are accurate (the curves for the representations (2) and (5) are visually identical).

To further demonstrate the convergence of the representation (5), Fig. 3(c) shows the relative error between the results obtained via (2) and (5) for the Green function G^{2D}. The error was defined as $\text{Error} = \left(\int |G^{2D}_{\text{Eq.(5)}}(\mathbf{r}) - G^{2D}_{\text{Eq.(2)}}(\mathbf{r})|^2 \, dx \Big/ \int |G^{2D}_{\text{Eq.(2)}}(\mathbf{r})|^2 \, dx \right)^{1/2}$. It is evident that the results converged very rapidly with an increase of the number of integration nodes. It was found that an optimal truncation value of k_t for the integration can be found for a given number of nodes. An interesting fact is that the convergence for $L = 1.2\lambda$ was better than for $L = 0.2\lambda$ and $L = 2.2\lambda$. The study is being pursued to investigate this point and to further improve the convergence. However, in all cases, the convergence is very good even for $|x|, |z|, \rho \to 0$ and even for large L (e.g. $L > 2\lambda$). Similar results were obtained for the convergence of G^{3D}. Similar results also were obtained for large $|z|, \rho$ (e.g. for $|z|, \rho \sim 3L$) with a slight increase of N_d.

5. Discussion and conclusions

Spectral representations for Green functions for 2D and 3D configurations with a 1D periodicity have been developed. The representations rely on the Green function expansions in terms of continuous longitudinal spectra. The Green functions are obtained in terms of a small number of direct source contributions, a small number of pole (Floquet mode) contributions, and a rapidly convergent integral, which can be evaluated using a small number of quadrature nodes. The presented schemes do not require evaluation of certain special functions as in the Ewald method, thus leading to an increased speed. They work seamlessly for small/vanishing or large $|z|, |x|, \rho$ as well as for small or large L. Moreover, they do not require explicitly defining the branch cuts associated with the Floquet mode wavenumbers.

The presented schemes can be extended to more complicated environments like layered media. For 2D problems these extensions are straightforward: One only adds in Eq. (3) a summation over the discrete spectrum of guided modes. Extensions can also be developed for 3D problems involving 2D periodicities. The presented ideas also can be used to calculate more complicated Green functions, e.g. Green function for a single source near an infinitely periodic structure. Such extensions will be reported elsewhere.

References

1. P.P. Ewald, “Die berechnung optischer und elektrostatischen gitterpotentiale,” *Ann. der Phys.* vol. 64, 1921, pp. 253–287, Translated by A. Cornell, *Atomics International Library*, 1964.

2. F. Capolino, D. R. Wilton and W. A. Johnson “Efficient computation of the 2-D Green’s function for 1-D periodic structures using the Ewald method,” *IEEE Trans. Antennas Propagat.*, vol. 53, 2005, pp. 2977-2984.

3. F. Capolino, D. R. Wilton and W. A. Johnson, “Efficient computation of the 3D Green’s function for the Helmholtz operator for a linear array of point sources using the Ewald method,” *J. Comp. Phys.*, vol. 223, 2007, pp. 250-261.

4. H. Rogier and D. De Zutter, “A fast converging series expansion for the 2-D periodic Green’s function based on perfectly matched layers,” *IEEE Trans. Microwave Theory Tech*., vol. 52, 2004, pp. 1199-1206.

5. H. Rogier, “New series expansions for the 3-D Green’s function of multilayered media with 1-D periodicity based on perfectly matched layers,” *IEEE Trans. Microwave Theory Tech*, vol. 55, 2007, pp. 1730-1738.

6. L. B. Felsen and N. Marcuvitz, *Radiation and Scattering of Waves*, New York: Prentice-Hall/IEEE Press, 1994.

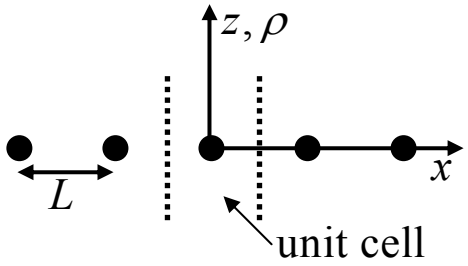

Fig. 1: Structure configuration

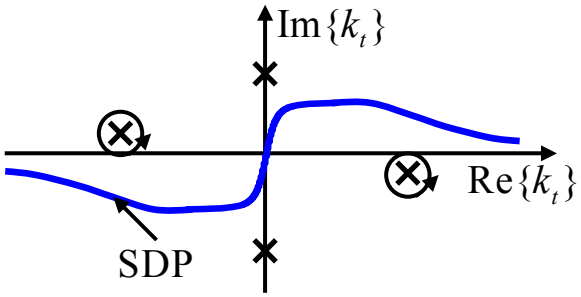

Fig. 2: Complex k_t plane. The SDP is chosen for $|z|=\rho=0$ corresponding to the saddle point at $k_z=0$.

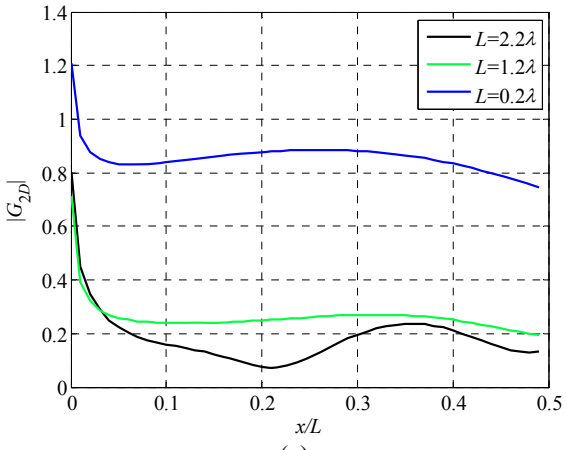

(a)

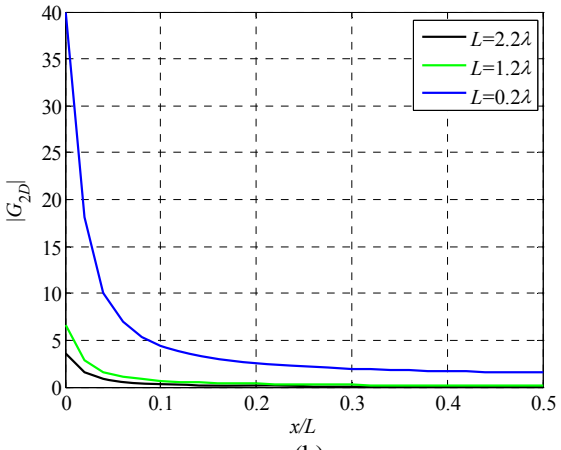

(b)

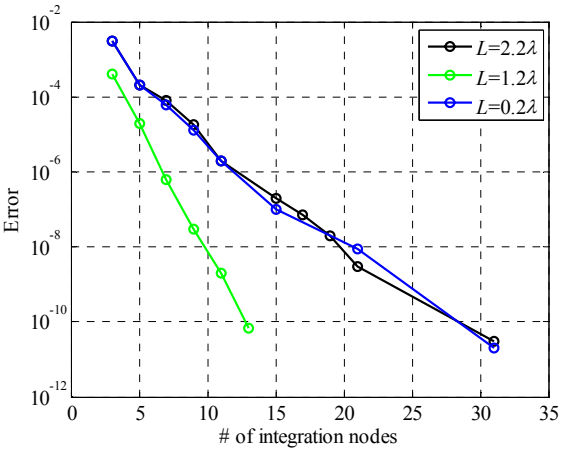

(c)

Fig. 3: Periodic Green functions and the relative error. (a) G^{2D} and (b) G^{3D} along the line $0.001L < x < 0.5L$ for $k_{x0} = (0.8 - 0.0001j)k$ for $|z| = \rho = 10^{-4}\lambda$. (c) The relative error for G^{2D}.